PIN1 inhibits ferroptosis in gastric cancer cells by regulating the CPEB1-GPX4 pathway

AORAN ZENG[1,2*], TAO WANG[3*], JIE SONG[1], LILI ZHU[4], LING CHEN[1], QI YUAN[5], YING JIANG[6], PING ZHANG[7,8], SHENGZHONG RONG[7,8] and JING WANG[1]

[1]Department of Biology, School of Basic Medical Sciences, Mudanjiang Medical University, Mudanjiang, Heilongjiang 157011, P.R. China; [2]School of Health and Nursing, Guangzhou Huali College (Jiangmen Campus), Jiangmen, Guangdong 529149, P.R. China; [3]Department of Ultrasound, The Second Affiliated Hospital of Mudanjiang Medical University, Mudanjiang, Heilongjiang 157000, P.R. China; [4]Department of Foreign Language Teaching and Researching, Mudanjiang Medical University, Mudanjiang, Heilongjiang 157011, P.R. China; [5]College of Life Science, Mudanjiang Medical University, Mudanjiang, Heilongjiang 157011, P.R. China; [6]Department of Biochemistry and Molecular Biology, Mudanjiang Medical University, Mudanjiang, Heilongjiang 157011, P.R. China; [7]Public Health School, Mudanjiang Medical University, Mudanjiang, Heilongjiang 157011, P.R. China; [8]Key Laboratory of Chronic Disease Etiology and Prevention and Treatment of Border Region in Heilongjiang, Mudanjiang Medical University, Mudanjiang, Heilongjiang 157011, P.R. China

Received November 6, 2025; Accepted May 11, 2026

DOI: 10.3892/or.2026.9156

Abstract. Ferroptosis, an iron-dependent form of programmed cell death, is a promising target for cancer therapy. Peptidyl-prolyl cis/trans isomerase 1 (PIN1), a member of the peptidyl-prolyl cis/trans isomerase family, is often overexpressed in cancer and contributes to tumor cell proliferation, survival and metastasis. The present study investigated whether PIN1 regulates ferroptosis in gastric cancer (GC). GC cell models with either PIN1 knockdown or overexpression were established and treated with the ferroptosis inducer erastin, followed by assessment of cell viability and proliferation rate using Cell Couting Kit-8 and colony formation assays, detection of PIN1 and cytoplasmic polyadenylation element binding protein 1 (CPEB1) expression via western blotting and reverse transcription-quantitative PCR, and evaluation of glutathione peroxidase 4 (GPX4) expression through immunofluorescence assay. Experimental results indicate that PIN1 depletion increases erastin-induced ferroptosis, as evidenced by increased levels of reactive oxygen species, malondialdehyde and intracellular free iron. PIN1 overexpression attenuates the erastin-induced ferroptotic response, as evidenced by decreased levels of ferroptosis-related biomarkers. Further analysis reveals that silencing PIN1 upregulates CPEB1, which, in turn, suppresses GPX4 expression. Simultaneous knockdown of CPEB1 reverses the ferroptosis-enhancing effect of PIN1 depletion. These mechanistic findings suggest that PIN1 promotes GPX4 expression by repressing CPEB1, thus inhibiting Erastin-induced ferroptotic cell death in GC. *In vivo* experiments further suggest that PIN1 knockdown significantly reduces the tumorigenic potential of GC cells. A novel PIN1-CPEB1-GPX4 axis was identified, in which PIN1 downregulates CPEB1 to mediate ferroptosis resistance. This axis represents a potential therapeutic target, as PIN1 knockout demonstrates significant tumor suppression in animal models. The present study identifies a novel PIN1-CPEB1-GPX4 regulatory axis that controls ferroptosis, suggesting its potential as a therapeutic target for advanced GC.

Correspondence to: Dr Jing Wang, Department of Biology, School of Basic Medical Sciences, Mudanjiang Medical University, 3 Tongxiang Street, Aimin, Mudanjiang, Heilongjiang 157011, P.R. China
E-mail: wangjing@mdjmu.edu.cn

Dr Shengzhong Rong, Public Health School, Mudanjiang Medical University, 3 Tongxiang Street, Aimin, Mudanjiang, Heilongjiang 157011, P.R. China
E-mail: sz_rong@yeah.net

*Contributed equally

Key words: PIN1, CPEB1, GPX4, ferroptosis, gastric cancer

Introduction

Gastric cancer (GC), a malignancy originating from the gastric epithelium, ranks as the 5th most common cancer globally and remains one of the leading tumors of the digestive system (1). Surgery remains the primary treatment approach, often combined with chemotherapy or radiotherapy. While effective chemotherapy can reduce recurrence rates and improve 5-year survival, the emergence of secondary drug resistance during long-term treatment presents a key obstacle in managing advanced GC. Therefore, the development of combination therapeutic strategies and the identification of novel chemotherapeutic targets to overcome chemoresistance have become urgent scientific priorities (2).

Ferroptosis is a regulated form of cell death characterized by iron-dependent accumulation of lipid peroxides, with distinct

morphological features and molecular mechanisms that differ from those of apoptosis and necrosis (3). Since the identification of ferroptosis by Dixon *et al* (4) in 2012, ferroptosis has gained increasing attention in studies associated with cancer, neurodegenerative disorders and ischemic injury (5,6). The rapid proliferation of tumor cells is frequently associated with disrupted lipid metabolism and iron homeostasis, making them particularly vulnerable to ferroptosis (7,8). Highly malignant or chemoradiotherapy-resistant tumor cells often depend heavily on antioxidant defense systems, further increasing their sensitivity to ferroptotic cell death (9,10). Therefore, targeting ferroptosis presents a potential therapeutic strategy for cancer treatment.

Peptidyl-prolyl cis/trans isomerase 1 (PIN1), a member of the PPIase family, regulates the function, activity and localization of target proteins by binding specifically to phosphorylated Ser/Thr motifs, thus inducing conformational changes (11). PIN1 is overexpressed in various tumor cell lines and is negatively associated with clinical prognosis (12). PIN1 has been implicated in chemoresistance across multiple types of cancer, including breast, liver and pancreatic cancer, with expression levels positively associated with the degree of drug resistance, highlighting its role as a key oncogenic factor (13,14). Previous studies have also associated PIN1 with ferroptosis. PIN1 inhibits ferroptosis by upregulating glutathione peroxidase 4 (GPX4), contributing to cisplatin resistance in cervical cancer cells, whereas PIN1 knockout reverses this resistance (15,16).

Cytoplasmic polyadenylation element-binding protein 1 (CPEB1), a member of the cpeb family, regulates essential cellular functions including proliferation, apoptosis, senescence and mitotic control, processes that carry out key roles in oncogenesis and tumor progression (17,18). In breast cancer, CPEB1 participates in the epithelial-mesenchymal transition (19), while in liver cancer, its downregulation contributes to increased chemoresistance and cellular stemness (20). Previous work demonstrated that overexpression of CPEB1 in GC cell lines HGC-27 and AGS elevates erastin-induced ferroptosis (21). PIN1 interacts with CPEB1 to catalyze the isomerization of specific phosphorylated residues, leading to ubiquitination-mediated degradation of CPEB (22). It has further been shown that PIN1 overexpression significantly shortens the half-life of CPEB1 in cells (23). However, the functional significance of this interaction in cancer biology, particularly in gastric cancer, remains unclear. PIN1 has been reported to suppress ferroptosis and promote chemoresistance, in part by upregulating GPX4 (15), whereas CPEB1 promotes ferroptosis by downregulating GPX4 expression in GC cells (21). These opposing effects raise an important question: Whether PIN1 inhibits ferroptosis in GC by targeting CPEB1 for degradation, alleviating CPEB1-mediated suppression of GPX4. Eucidating this potential PIN1-CPEB1-GPX4 axis is essential for understanding ferroptosis resistance in GC.

The present study aims to investigate the regulatory role of PIN1 in ferroptosis in gastric cancer, focusing on elucidating the underlying mechanism by which PIN1 suppresses ferroptotic cell death through CPEB1-dependent upregulation of GPX4.

Materials and methods

Chemical reagents. Ferrostatin-1 (Fer-1; cat. no. HY-100579) was obtained from MedChemExpress and dissolved in DMSO to prepare a 10 mM stock solution. Erastin, a classic ferroptosis inducer (cat. no. SC0224; Beyotime Biotechnology) was prepared as a 20 mM stock solution in DMSO.

Cell culture. The GC cell line HGC-27 was purchased from Beyotime Biotechnology, while the GC cell line AGS and the gastric epithelial cell line GES-1 were provided by Suzhou Haixing Biosciences Co., Ltd. AGS cells were cultured in Ham's F-12K medium (Thermo Fisher Scientific, Inc.) supplemented with 10% fetal bovine serum (FBS; Anhui Gezhe Biotechnology Co., Ltd.). HGC-27 and GES-1 cells were cultured in RPMI-1640 medium (Thermo Fisher Scientific, Inc.) with 10% FBS from the same supplier. All cell lines were authenticated and tested negative for mycoplasma contamination. All cell lines were maintained under standard culture conditions (37˚C; 5% CO_2; humidified atmosphere). Cells were treated with 10 μM Erastin or 1 μM Fer-1 at 37˚C for 24 h.

Cell viability assay and colony formation assay. Cellular viability was evaluated using the Cell Counting Kit-8 (CCK-8; cat. no. C0041; Beyotime Biotechnology). GC cells were seeded in 96-well plates at a density of $5x10^3$ cells per well and exposed to 10 μM erastin at 37˚C for 24 h, after which the CCK-8 assay was performed according to the manufacturer's protocol with a 2-h incubation at 37˚C.

For the colony formation assay, transfected HGC-27 and AGS cells were seeded at $1x10^3$ cells per well in 6-well plates and incubated overnight at 37˚C. The erastin-treated group was exposed to a final concentration of 10 μM Erastin at 37˚C for 24 h. The culture medium was changed every 3 days until visible colonies appeared. After a 14-day incubation period, the cells were fixed with 4% paraformaldehyde at room temperature for 15 min and stained with 0.1% crystal violet at room temperature for 30 min. Colonies containing ≥50 cells were counted manually under a light microscope.

Small interfering (si)RNA transfection. Knockdown of PIN1 and CPEB1 was performed by transfection of specific small interfering RNAs (siRNAs) at a final concentration of 50 nM using Lipofectamine® 3000 reagent (Invitrogen; Thermo Fisher Scientific, Inc.), according to the manufacturer's instructions. After incubation at 37˚C for 4 h, the transfection medium was replaced with fresh complete medium, and cells were cultured for an additional 48 h before subsequent experiments. The sequences of the siRNA duplexes (5' to 3') used are listed in Table I. All siRNAs were synthesized by Beyotime Biotechnology.

Plasmid transfection. Overexpression of PIN1 and CPEB1 was achieved by transfection of plasmid vectors. The PIN1 overexpression plasmid (pcDNA3.1-PIN1) was obtained as a glycerol stock from Vertex Pharmaceuticals (Europe) Limited. The CPEB1 overexpression plasmid (pcDNA3.1-CPEB1) was obtained as a glycerol stock from Haixing Biosciences. Both plasmids were constructed using the pcDNA3.1(+) vector backbone. Plasmids were extracted and purified prior to transfection. Cells were seeded in 6-well plates and transfected with 2 μg of plasmid DNA at 70-80% confluence using Lipofectamine® 3000 reagent (Invitrogen; Thermo Fisher Scientific Inc.) according to the manufacturer's instructions.

Table I. Small interfering RNA sequences used in the present study.

Target	Sence sequence (5'-3')	Antisense sequence (5'-3')
PIN1	CAGCAGCAGUGGUGGCAAATT	UUUGCCACCACUGCUGCUGTT
CPEB1	GGGUAUUAGCCGACAGUAATT	UUACUGUCGGCUAAUACCCTT
Negative control	UUCUCCGAACGUGUCACGUTT	ACGUGACACGUUCGGAGAATT

PIN1, peptidyl-prolyl cis/trans isomerase 1; CPEB1, cytoplasmic polyadenylation element-binding protein 1.

Table II. Reverse transcription primer sequences.

Gene	NCBI mRNA ID	Forward primer sequence (5'-3')	Reverse primer sequence (5'-3')
GAPDH	NM_002046.7	GAGAAGGCTGGGGCTCATTT	TGCTGATGATCTTGAGGCTGT
PIN1	NM_006221.4	CCGCAGCTCAGGCCG	CTGCCCGTTTTTGCCACC
CPEB1	NM_030594.5	TCGGTGCTCTGCATGGAATG	AGTCACACGACCAGAACCAAT

PIN1, peptidyl-prolyl cis/trans isomerase 1; CPEB1, cytoplasmic polyadenylation element-binding protein 1.

After incubation at 37˚C for 4 h, the transfection medium was replaced with fresh complete medium. An empty pcDNA3.1(+) vector was used as the negative control. At 48 h post-transfection, successful overexpression was confirmed by western blotting (Fig. S1). For co-overexpression experiments, cells were co-transfected with equal amounts (2 μg each) of pcDNA3.1-PIN1 and pcDNA3.1-CPEB1 using the same protocol.

Reverse transcription-quantitative PCR (RT-qPCR) analysis. Total RNA was extracted from HGC-27 and AGS GC cells following siRNA-mediated PIN1 knockdown and plasmid-based overexpression, after 24-h treatment with 10 μM Erastin, to validate the regulatory effects of PIN1 on CPEB1 expression and erastin-induced ferroptosis. Total RNA was extracted using the Total RNA Extraction Kit (cat. no. M5101; Suzhou Xinsaimei Biotechnology Co., Ltd.). RT was performed using theFirst Strand cDNA Synthesis Kit (cat. no. D7168M; Beyotime Biotechnology). qPCR was conducted using commercially designed and validated primer pairs (Beyotime Biotechnology), cDNA templates and BeyoFast™ SYBR Green qPCR Mix (2x; Low ROX; cat. no. D7262; Beyotime Biotechnology). RT-qPCR was performed on an Applied Biosystems 7500 Real-Time PCR System (Thermo Fisher Scientific, Inc.). The thermal cycling conditions were as follows: 95˚C for 2 min, followed by 40 cycles of 95˚C for 15 sec and 60˚C for 25 sec. Relative mRNA levels were calculated using the $2^{-\Delta\Delta Cq}$ method (24). All primer pairs were purchased from Beyotime Biotechnology. All primer pairs were purchased from Beyotime Biotechnology. The NCBI mRNA IDs and primer sequences are listed in Table II.

Western blotting. Proteins were extracted from GC cells following siRNA-mediated PIN1 knockdown and plasmid-based overexpression, after 24-h treatment with 10 μM erastin, to validate the regulatory effects of PIN1 on CPEB1 expression and erastin-induced ferroptosis. Cellular proteins were extracted from GC cells using Beyotime lysis buffer (Beyotime Biotechnology) and protein concentration was determined using the BCA assay kit (Beyotime Biotechnology). Equal amounts of protein (30 μg) were separated on 12% SDS-PAGE gels and transferred to PVDF membranes (Biosharp Life Sciences) via electroblotting. Membranes were blocked for 1 h at room temperature with 5% skimmed milk and then incubated overnight at 4˚C with the following primary antibodies: CPEB1 (1:2,000; cat. no. 13274-1-AP; Proteintech Group, Inc.), PIN1 (1:5,000; cat no. 10495-1-AP; Proteintech Group, Inc.), GPX4 (1:500; cat. no. AF7020; Beyotime Biotechnology) and GAPDH (1:10,000; cat. no. AG0122; Beyotime Biotechnology). Membranes were then incubated with horseradish peroxidase (HRP)-conjugated secondary antibodies (1:1,000; cat. no. AG8064; Beyotime Biotechnology) for 1 h at room temperature. Protein bands were visualized using an ECL substrate (cat. no. P0018S; Beyotime Biotechnology) and imaged with a ChemiDoc XRS+ system (Bio-Rad Laboratories, Inc.). Quantification was performed using ImageJ software (version 1.53a; National Institutes of Health) with normalization to GAPDH.

Detection of lipid reactive oxygen species (ROS), malondialdehyde (MDA) and ferrous iron (Fe^{2+}). Lipid ROS levels in GC cells and tumor tissues were measured using the ROS Assay Kit (cat. no. S0033S; Beyotime Biotechnology). After Erastin treatment for 24 h, cells were incubated with 5 μM DCFH-DA at 37˚C for 30 min, followed by fluorescence microscopy observation. For MDA and Fe^{2+} quantification, $2x10^7$ cells per group were lysed after erastin treatment for 24 h. MDA content and Fe^{2+} levels were quantified using the MDA Assay Kit (cat. no. S0131S; Beyotime Biotechnology) and the Iron Colorimetric Assay Kit (cat. no. E1046; Beijing Applygen Technologies Inc.), respectively, according to the manufacturers' instructions.

Co-immunoprecipitation (Co-IP) and western blot analysis. Protein-protein interactions were analyzed by Co-IP using a Protein A magnetic bead-based immunoprecipitation kit (cat. no. G2209-50Tl; Wuhan Servicebio Technology Co., Ltd.) according to the manufacturer's instructions. HGC-27 cells were harvested by trypsin digestion and lysed in RIPA lysis buffer (cat. no. P0013C; Beyotime Biotechnology) supplemented with a protease inhibitor cocktail. After centrifugation at 12,000 x g for 15 min at 4˚C, the supernatant was collected and protein concentration was determined. For each IP reaction, 500 μg of protein lysate were incubated overnight at 4˚C with an anti-CPEB1 antibody (1:150; cat. no. 13274-1-AP; Proteintech Group, Inc.) or control mouse IgG (cat. no. A7028; Beyotime Biotechnology). Protein A magnetic beads were then added and incubated for 2 h at room temperature. After three washes with 1x TBS buffer, bound proteins were eluted by boiling in 1X SDS loading buffer for 5 min and subjected to western blot analysis using the same procedure as aforementioned with antibodies against PIN1 and CPEB1.

Xenograft tumor model in nude mice. All animal procedures were approved by the Institutional Animal Care and Use Committee (IACUC) of Mudanjiang Medical University, Mudanjiang, China (approval no. IACUC-20240719-079). A total of 18 healthy male nude mice (5 weeks old, weighing 18-20 g) were obtained from Beijing Vital River Laboratory Animal Technology Co., Ltd. and randomly assigned to three groups (n=6 per group): Group A, knockout negative control (koNC) + Vehicle; Group B, koNC + Erastin and Group C, koPIN1 + Vehicle.

The mice were housed in a controlled environment with a 12-h light/dark cycle, a temperature of 22±1˚C and humidity maintained at 45-55%, with *ad libitum* access to food and water. Their health and behavior were assessed daily. Before implantation, PIN1 knockout in the HGC-27 cells was confirmed by western blot analysis. Logarithmic-phase PIN1-knockout GC cells or control cells ($5x10^6$) were then subcutaneously injected. When the tumor volume reached 100 mm^3, Group B was treated with daily intraperitoneal injections of erastin (60 mg/kg). Tumor size was monitored by measuring the tumor diameter (D) with digital calipers every 3 days. The humane endpoint was defined as a tumor diameter >15 mm, tumor volume >800 mm^3, tumor ulceration or body weight loss >20%. No animals reached these endpoints during the study. Tumor volume (V) was calculated using the formula for a sphere: $V=4/3x\ \pi\ x\ (D/2)^3$. The maximum tumor diameter and volume observed during the study were 10.8 mm and ~650 mm^3, respectively, which were well within the humane endpoints of the approved protocol. The experiment lasted 15 days. At the study's conclusion, mice were euthanized by cervical dislocation following deep anesthesia induced by inhalation of 3% isoflurane (air as carrier gas). Mortality was confirmed by the absence of respiration, heartbeat and corneal reflex. Tumor tissues were then collected for analysis.

Immunohistochemistry. A total of 27 patients with gastric cancer (18 men and 9 women; median age 68 years, range 37-89 years) who underwent radical gastrectomy were included in the present study. All surgical specimens were collected between March, 2023 and December, 2023, in accordance with the approved ethics protocol (approval no. 2023-MYGZR01). Their paraffin-embedded tumor tissues and matched adjacent normal tissues were used for immunohistochemical analysis.

Immunohistochemical staining was conducted on 27 pairs of pathologically confirmed paraffin-embedded GC tissues and matched adjacent normal tissues. Tissue sections were deparaffinized in xylene (three changes, 5 min each) and rehydrated through a graded ethanol series (100, 95, 85 and 75%, 5 min each) to distilled water. Antigen retrieval was performed in citrate buffer (pH 6.0) by microwave heating at 95-100˚C for 30 min, followed by washing with PBS. Endogenous peroxidase activity was blocked with 3% hydrogen peroxide at room temperature for 10 min. Sections were then blocked with 5% goat serum at room temperature for 1 h to reduce non-specific binding. After blocking, sections were then incubated with a primary antibody against PIN1 (1:200; cat no. 10495-1-AP, Proteintech Group, Inc.) at 4˚C overnight, followed by an HRP-conjugated secondary antibody for 1 h at room temperature. The signal was visualized using a 3,3'-diaminobenzidine substrate kit (cat no. G1212; Wuhan Servicebio Technology Co., Ltd.) and nuclei were counterstained with hematoxylin at room temperature for 2 min.

Quantitative analysis of PIN1 expression was performed using image analysis software (version 1.53a; National Institutes of Health). The staining intensity was assessed by calculating the H-score, defined as: H-Score=[1 x (Area_weak/Total_area) + 2x (Area_moderate/Total_area) + 3x (Area_strong/Total_area)] x100.

Bioinformatics analysis. Bioinformatic analyses of GC and adjacent normal tissues were conducted using the GSE220917 dataset (accession no. GSE220917) from the Gene Expression Omnibus (GEO) database (https://www.ncbi.nlm.nih.gov/geo/) and The Cancer Genome Atlas Stomach Adenocarcinoma (TCGA-STAD) dataset from TCGA. All statistical analyses were performed in R (version 4.2.0; R Core Team). For the GSE220917 RNA-sequencing (RNA-seq) data, read counts were normalized using the DESeq2 package and differentially expressed genes were identified with DESeq2 (v1.36) using |log2(Fold Change)|>1 and false discovery rate (FDR) <0.05. Pearson correlation analysis (P<0.05) was used to assess the correlation between PIN1 and CPEB1 expression. Kaplan-Meier survival curves were generated with the R survival package (v3.3.3) and group differences were evaluated using the Log-rank test. Gene Set Enrichment Analysis (GSEA v4.3.2) was conducted using the MSigDB C5 (GO gene sets) database. Pathways with FDR <0.25 and P<0.05 were considered significantly enriched.

Receiver operating characteristic (ROC) curve analysis was performed using TCGA-STAD data. ROC curves for PIN1 and CPEB1 were generated from their gene expression levels, and the area under the curve (AUC) was calculated to assess their diagnostic performance.

Statistical analysis. Data are presented as the mean ± SD from at least three independent experiments. Statistical analyses were performed using GraphPad Prism 8 (Dotmatics). Differences between two paired groups were evaluated using a paired Student's t-test. Comparisons between two unpaired groups were assessed using an unpaired Student's t-test. Comparisons among multiple groups were performed

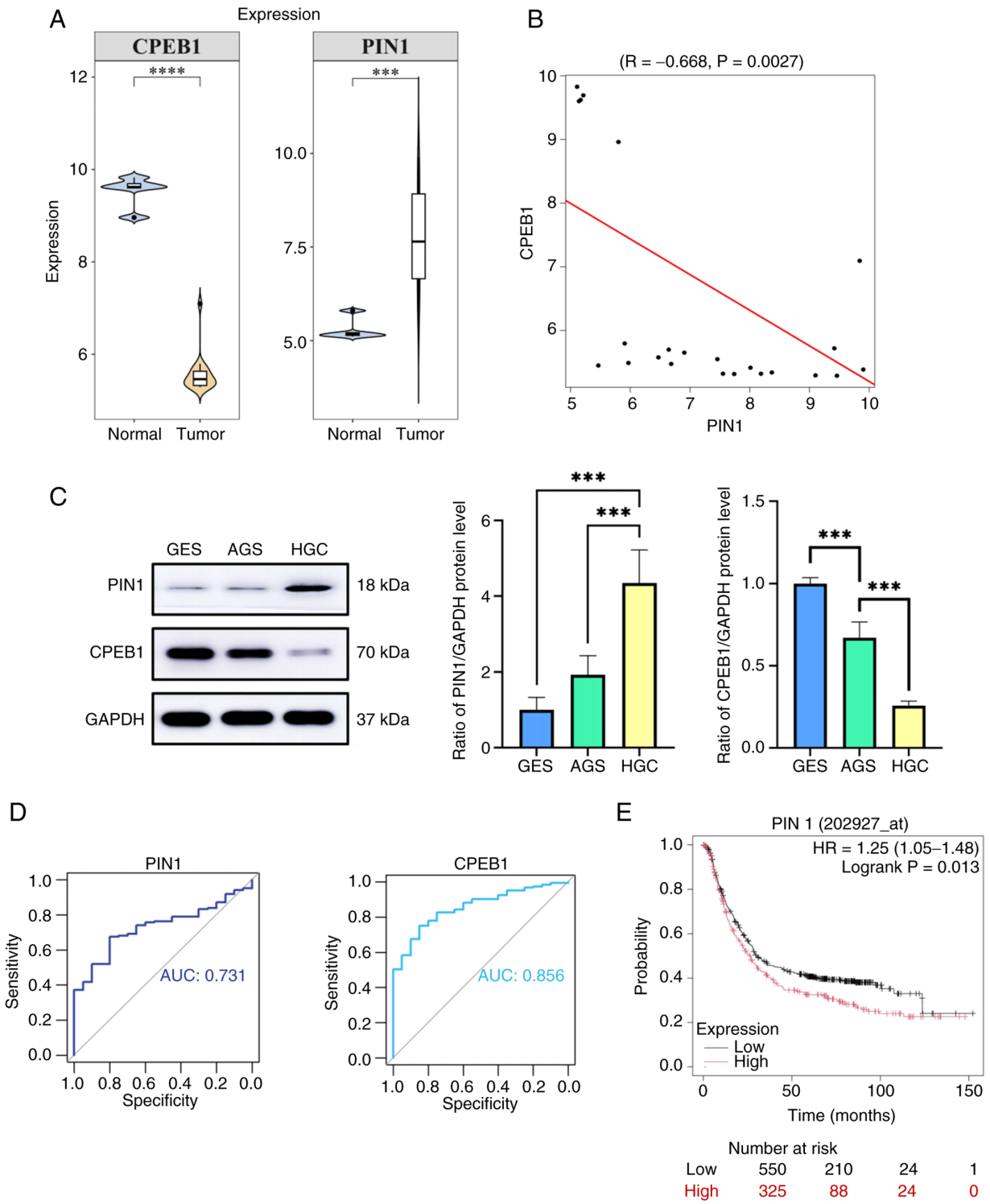

Figure 1. Expression of PIN1 and CPEB1 in GC. (A) Bioinformatics analysis of PIN1 and CPEB1 mRNA levels in GC and matched adjacent normal tissues. (B) Correlation analysis of PIN1 and CPEB1 mRNA expression in GC tissues (R=-0.668, P=0.0027). (C) Western blot analysis of PIN1 and CPEB1 protein levels in the normal gastric epithelial cell line GES-1 and GC cell lines HGC-27 and AGS. (D) Receiver operating characteristic curves for PIN1 and CPEB1 based on the TCGA-STAD dataset. (E) Kaplan-Meier survival analysis of patients with GC stratified by PIN1 expression levels (P=0.013). Data are expressed as mean ± SD (n=3). ***P<0.001, ****P<0.0001. PIN1, peptidyl-prolyl cis/trans isomerase 1; CPEB1, cytoplasmic polyadenylation element-binding protein 1; GC, gastric cancer; AUC, area under the curve.

using one-way ANOVA followed by Tukey's post hoc test. Categorical data (such as the association between PIN1 expression and clinicopathological features) were analyzed using Fisher's exact test. P<0.05 was considered to indicate a statistically significant difference.

Results

PIN1 is highly expressed in GC cells and tissues. To investigate the regulatory role of PIN1 in GC development, bioinformatics analysis was performed using the GSE220917 dataset from the

Table III. PIN1 H-score in paired gastric cancer and normal tissues.

Group	n	H-score, Mean ± SD	P-value
Tumor tissue	27	37.73±23.41	<0.001
Adjacent normal tissue	27	21.60±11.87	-

P-value was derived from a paired t-test (t=3.914; df=26). PIN1, peptidyl-prolyl cis/trans isomerase 1.

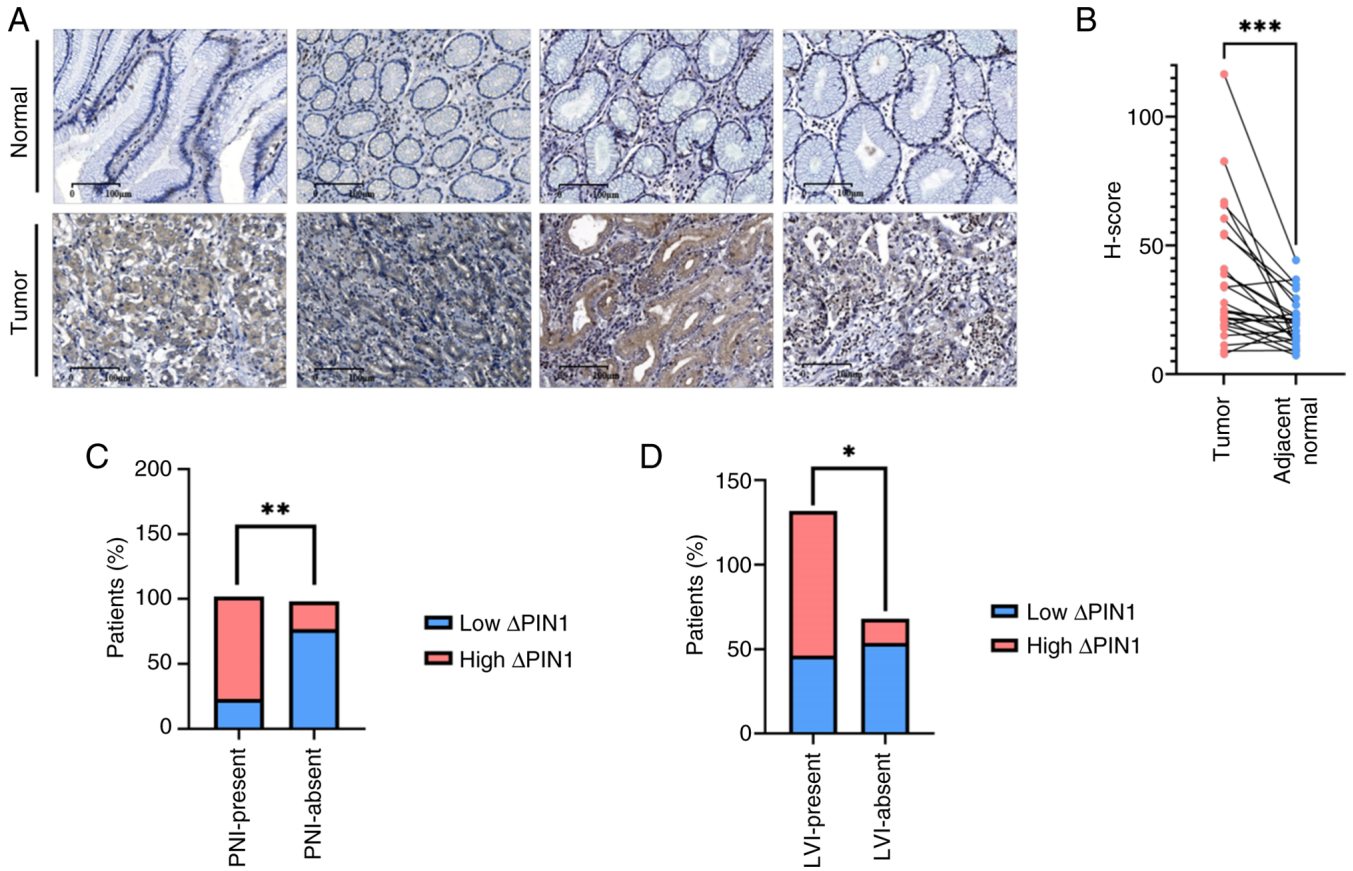

Figure 2. Expression of PIN1 in GC tissues and its clinical relevance. (A) Representative immunohistochemical staining images of PIN1 in GC and adjacent normal tissues. (B) Scatter plot comparing PIN1 H-scores in 27 paired GC tissues and adjacent normal tissues (paired t-test). Patients (%) with (C) lymphovascular invasion (P=0.0073) and (D) perineural invasion (P=0.0461) in the low and high ΔPIN1 groups (Fisher's exact test). ΔPIN1 is defined as the difference in PIN1 H-score between tumor and adjacent tissue. Data are presented as mean ± SD. *P<0.05; **P<0.01; ***P<0.001. PIN1, peptidyl-prolyl cis/trans isomerase 1; GC, gastric cancer.

GEO database. Comparative evaluation of PIN1 and CPEB1 expression between malignant gastric tissues and matched adjacent normal specimens revealed significantly increased levels of PIN1 and decreased levels of CPEB1 in tumor samples (Fig. 1A). Correlation analysis further demonstrated a negative association between PIN1 and CPEB1 mRNA expression in GC tissues (Fig. 1B).

The findings were further validated through *in vitro* experiments. Western blot analysis revealed significantly elevated PIN1 protein levels in GC cell lines (HGC-27 and AGS) compared with the normal gastric epithelial cell line GES-1, accompanied by an inverse relationship with CPEB1 expression (Fig. 1C).

To assess the ability of PIN1 and CPEB1 to distinguish GC samples from controls, ROC curve analysis was performed using the TCGA-STAD dataset. The AUC was 0.731 for PIN1 and 0.856 for CPEB1 (Fig. 1D). Further evaluation at optimal cut-off values showed that both genes exhibited robust diagnostic accuracy, as summarized in Table III. With both AUC values >0.7, these results indicate a good diagnostic performance for both genes in discriminating GC from normal tissues. Kaplan-Meier survival analysis showed that patients with high PIN1 expression had significantly reduced overall survival (Fig. 1E). These results underscore the pivotal role of PIN1 in the progression of GC.

Clinical association of PIN1 overexpression with aggressive features in patients with GC. To further evaluate the clinical relevance of PIN1, immunohistochemistry was performed on 27 paired GC tissues and matched adjacent normal tissues.

Table IV. PIN1 expression and clinicopathological features in gastric cancer.

Characteristics	Total	PIN1 high expression, n (%)	P-value	Odds ratio (95% CI)
Age				
<65 years	7	5 (71.4)	0.371	-
≥65 years	16	7 (43.8)		
Sex				
Men	16	8 (50.0)	1.000	-
Women	7	4 (57.1)		
Vascular tumor thrombus				
Absent	6	1 (16.7)	0.069	9.17 (0.86-97.60)
Present	17	11 (64.7)		
Neural invasion				
Absent	7	1 (14.3)	0.027	13.20 (1.24-140.50)
Present	16	11 (68.8)		
Lymph node metastasis				
Absent	6	1 (16.7)	0.069	9.17 (0.86-97.60)
Present	17	11 (64.7)		

Table V. Diagnostic performance of PIN1 and CPEB1 based on ROC curve analysis.

Gene	AUC	Accuracy	Sensitivity	Specificity
PIN1	0.731	0.779	0.809	0.765
CPEB1	0.856	0.834	0.834	0.800

AUC, area under the curve; ROC, receiver operating characteristic; PIN1, peptidyl-prolyl cis/trans isomerase 1; CPEB1, cytoplasmic polyadenylation element-binding protein 1.

Quantitative H-score analysis showed that PIN1 expression was significantly increased in GC tissues when compared with corresponding normal tissues (Fig. 2A and B; Table IV). To assess tumor-specific overexpression, ΔPIN1 was calculated as the difference between tumor and adjacent tissue H-scores, and patients were stratified into high- and low-ΔPIN1 groups based on the median value. High ΔPIN1 was significantly associated with lymphovascular invasion and perineural invasion (Fig. 2C and D; Table V). These results indicate that PIN1 overexpression may be associated with increased local invasiveness and aggressive pathological behaviors in GC.

PIN1 inhibits erastin-induced ferroptosis in GC cells. To elucidate the functional role of PIN1 in gastric carcinogenesis, GSEA was performed, focusing on the five most significantly enriched pathways. The analysis revealed associations between PIN1 and the 'sequestering of metal ion' and 'negative regulation of execution phase of apoptosis' pathways (Fig. 3A). Given that ferroptosis is an iron-dependent form of programmed cell death, these findings suggest that PIN1 may play a regulatory role in tumor cell ferroptosis.

PIN1-knockdown and overexpression cell lines were established using HGC-27 and AGS cells. Successful transfection was confirmed by western blotting (Fig. 3B and C) and RT-qPCR (Fig. 3D and E). Cell viability assays (CCK-8) and colony formation assays showed that erastin induced cell death in GC cells, which was reversed by the ferroptosis inhibitor Fer-1. PIN1 knockdown increased Erastin-induced ferroptosis, whereas PIN1 overexpression attenuated this effect (Fig. 4A-D). These findings suggest that PIN1 may suppress erastin-induced ferroptosis in GC cells.

Further analysis of ferroptosis-related markers showed that erastin treatment increased MDA and Fe^{2+} levels in GC cells compared with the untreated control group. PIN1 knockdown further elevated intracellular MDA and Fe^{2+} levels, whereas PIN1 overexpression reduced their accumulation (Fig. 4E-H). DCFH-DA fluorescence probe assays indicated that PIN1 knockdown upregulated ROS levels, while PIN1 overexpression suppressed ROS production (Fig. 4I and J). These results demonstrate that PIN1 may modulate erastin-induced ferroptosis in GC cells, acting as an inhibitory factor. Modulating PIN1 expression, whether by knockdown or overexpression, even in the absence of erastin, was sufficient to alter key ferroptosis markers, further supporting its role as a negative regulator of ferroptotic cell death in GC.

PIN1 downregulates CPEB1 expression in GC cells. To examine whether PIN1 regulates CPEB1 expression in GC cells, cell lines with siPIN1, siPIN1 + siCPEB1, ovPIN1 and ovPIN1 + ovCPEB1 were generated. RT-qPCR (Fig. 5A-D) and western blotting (Fig. 5I and J) revealed that PIN1 knockdown led to increased CPEB1 protein expression levels, whereas PIN1 overexpression resulted in decreased CPEB1 expression levels, indicating that PIN1 may negatively regulate CPEB1 in GC cells. Immunofluorescence analysis and quantitative measurement of GPX4 expression levels showed that PIN1 upregulates GPX4, whereas CPEB1 overexpression counteracts

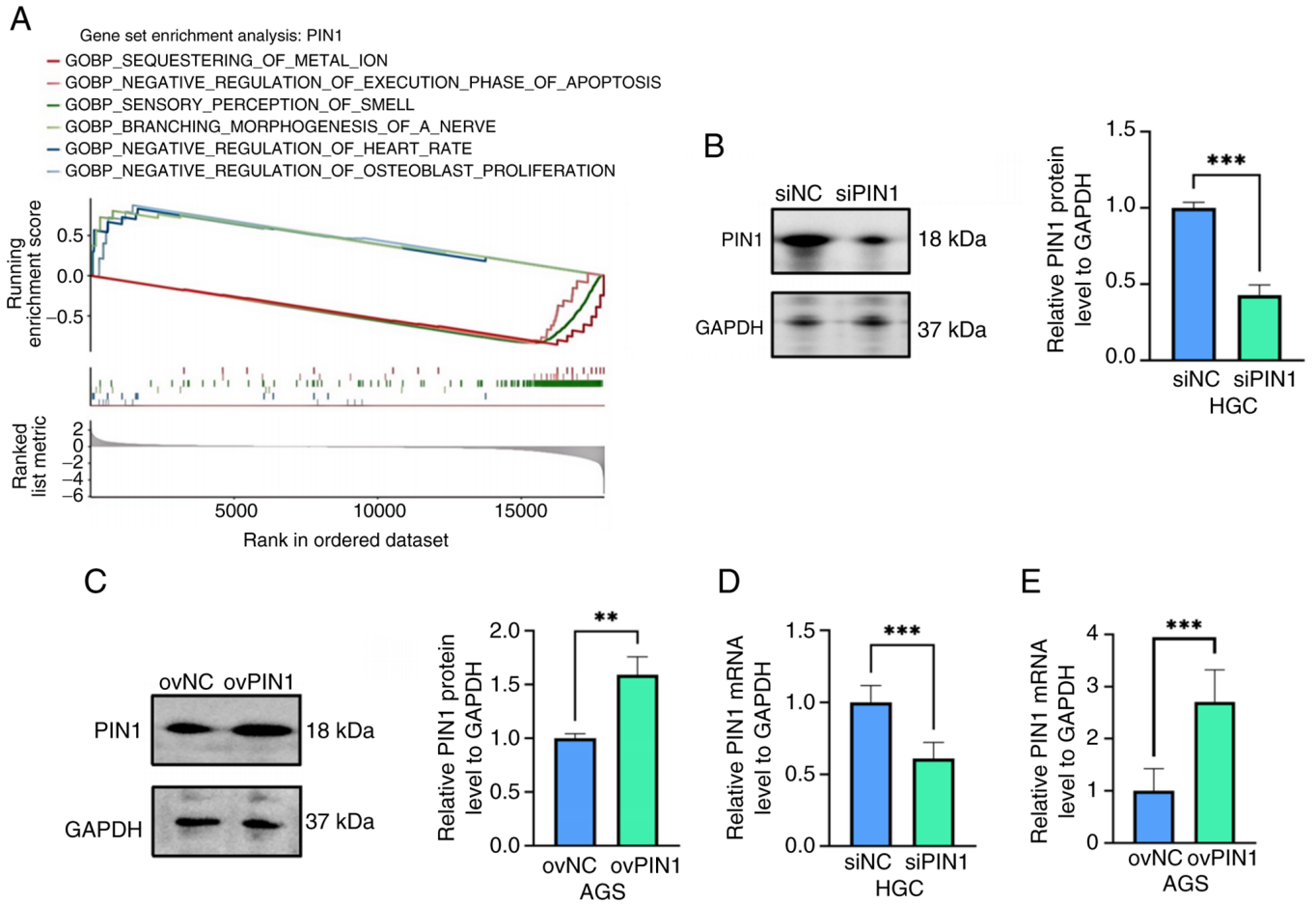

Figure 3. Regulatory role of PIN1 in ferroptosis of GC cells. (A) Gene set enrichment analysis. (B) Representative western blotting images and semi-quantitative analysis of PIN1 expression in PIN1-knockdown HGC-27 cells. (C) Representative western blotting images and semi-quantitative analysis of PIN1 expression in PIN1-overexpressionAGS cells. Reverse transcription-quantitative PCR analysis of PIN1 expression levels in (D) PIN1-knockdown HGC-27 and (E) PIN1-overexpression AGS cells. Data are expressed as mean ± SD (n=3). **P<0.01; ***P<0.001. PIN1, peptidyl-prolyl cis/trans isomerase 1; GC, gastric cancer; si, small interfering; ov, overexpression.

this effect (Fig. 5E-H). These findings suggest that PIN1 may promote GPX4 expression in GC cells by suppressing CPEB1.

PIN1 regulates ferroptosis in GC cells by inhibiting CPEB1. To determine whether PIN1 modulates ferroptosis through CPEB1, HGC-27 cells with concurrent knockdown of PIN1 and CPEB1 were treated with erastin. Ferroptosis-related markers were then analyzed. Compared with the siPIN1 + erastin group, the siPIN1 + siCPEB1 + erastin group showed reduced intracellular levels of MDA and Fe^{2+} (Fig. 6E and G), along with reduced ROS levels (Fig. 6I).

To further investigate how PIN1 regulates CPEB1, AGS cell lines overexpressing either PIN1 or CPEB1 were established. After exposing the cells to erastin, cell viability was assessed using CCK-8 assays and proliferative potential was evaluated through colony formation assays. The results showed that the ovPIN1 + ovCPEB1 + erastin group showed decreased cell survival and proliferation compared with the ovPIN1 + erastin group (Fig. 6B and D). Analysis of ferroptosis-related markers revealed elevated levels of ROS, MDA and Fe^{2+} in the ovPIN1 + ovCPEB1 + erastin group compared with the ovPIN1 + erastin group (Fig. 6F, H and G). These findings indicate that PIN1 regulates ferroptosis in GC cells by inhibiting CPEB1.

PIN1 interacts with CPEB1 and regulates its proteasome-dependent turnover. To elucidate the molecular basis for PIN1-mediated regulation of CPEB1, the present study first confirmed the expression of both proteins in the HGC-27 cells used for interaction experiments (Fig. 7A). Endogenous interaction was then examined by Co-IP. PIN1 was specifically co-precipitated using a CPEB1 antibody, while only a background signal was detected with the IgG control (Fig. 7B), demonstrating a direct interaction between PIN1 and CPEB1 in GC cells.

Next, the present study assessed whether CPEB1 stability is regulated by the ubiquitin-proteasome system. Treatment with the proteasome inhibitor MG132 resulted in a significant, time-dependent accumulation of CPEB1 protein compared with untreated controls (Fig. 7C), indicating that CPEB1 levels are tightly controlled by proteasomal degradation.

PIN1 knockdown inhibits tumor growth in GC xenografts. To assess the role of PIN1 in regulating ferroptosis *in vivo*, a xenograft tumor model was created using HGC-27 cells in nude mice. Western blot analysis confirmed PIN1 knockout in the cells before implantation (Fig. 8A). The mice were grouped into koNC, koNC + erastin and koPIN1 categories. Erastin

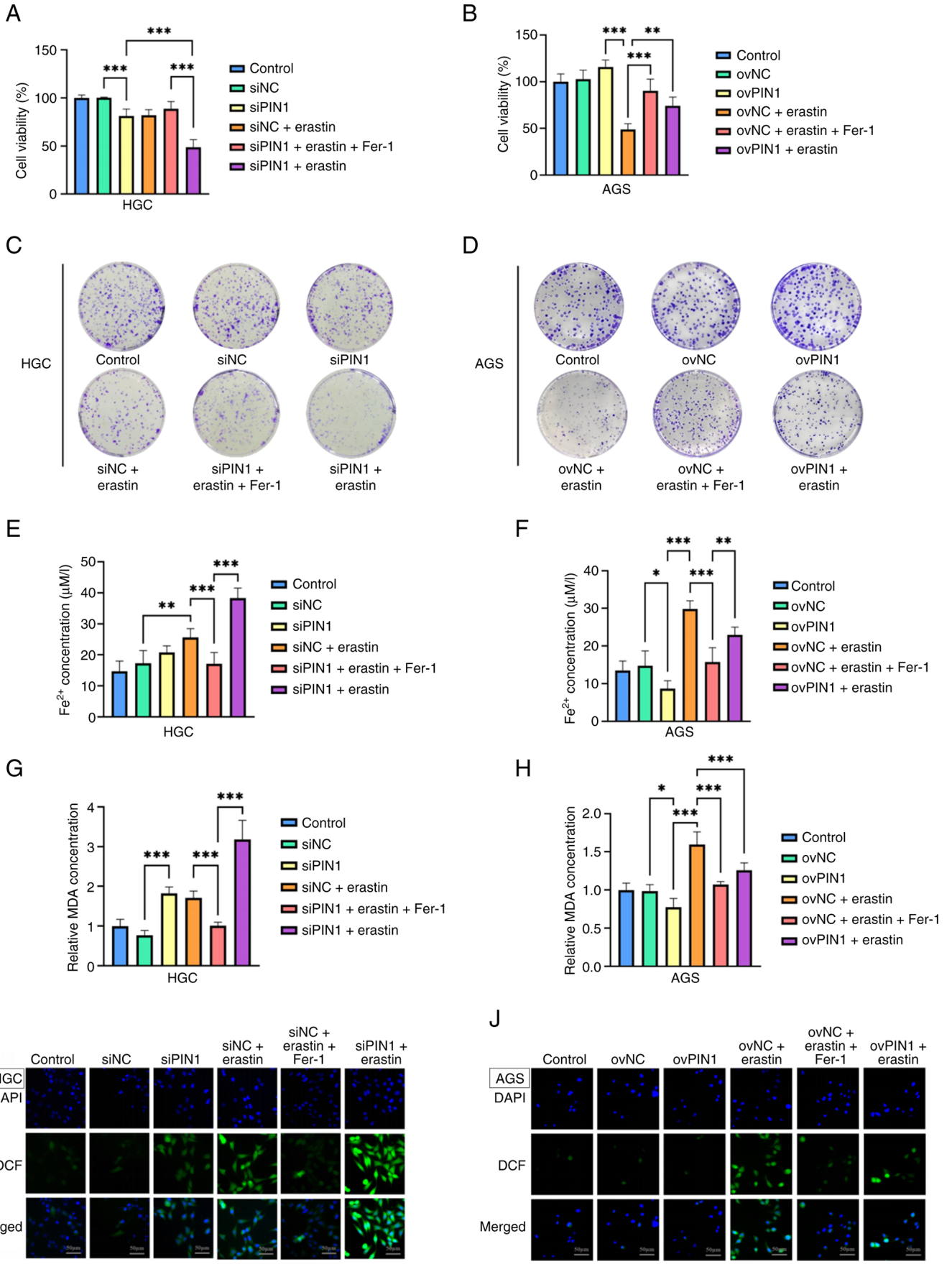

Figure 4. Regulation of erastin-induced ferroptosis by PIN1. Cell viability of (A) HGC-27 and (B) AGS GC cells. Colony formation assay in (C) HGC-27 and (D) AGS GC cells. Ferrous ion (Fe^{2+}) levels in (E) HGC-27 and (F) AGS cells. MDA levels in (G) HGC-27 and (H) AGS cells. Reactive oxygen species detection using 2',7'-dichlorodihydrofluorescein diacetate (DCFH-DA) fluorescence microscopy in (I) HGC-27 and (J) AGS cells. Data are presented as mean ± SD (n=3). *P<0.05; **P<0.01; ***P<0.001. PIN1, peptidyl-prolyl cis/trans isomerase 1; GC, gastric cancer; si, small interfering; ov, overexpression; NC, negative control; MDA, malondialdehyde.

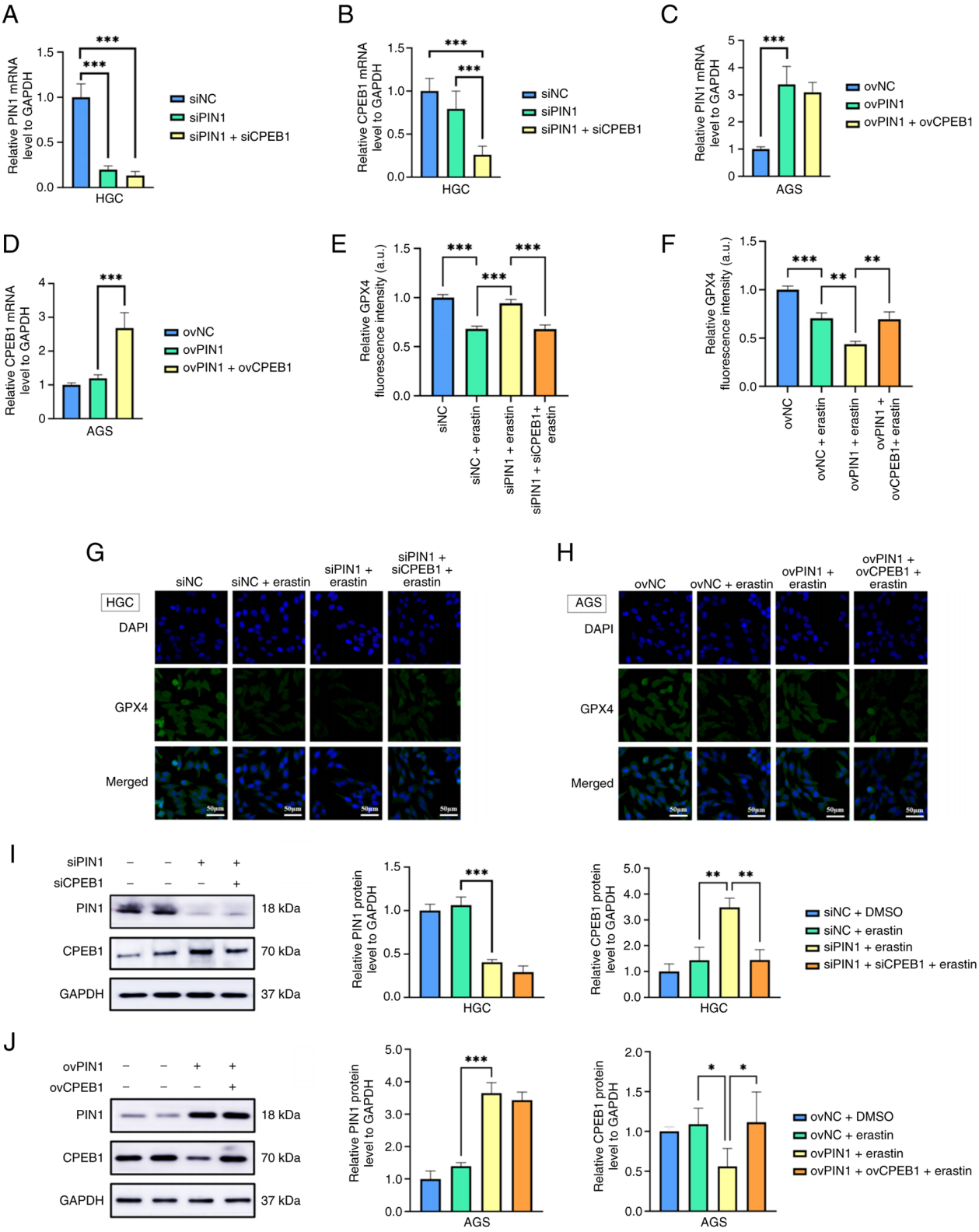

Figure 5. Downregulation of CPEB1 by PIN1 in GC cells. (A and B) RT-qPCR of (A) PIN1 and (B) CPEB1 in PIN1 and CPEB1 knockdown HGC-27 cells. RT-qPCR analysis of (C) PIN1 and (D) CPEB1 in PIN1 and CPEB1 overexpressed AGS cells. (E) Immunofluorescence staining for GPX4 in HGC-27 cells. (F) Immunofluorescence staining for GPX4 in AGS cells. (G) Quantitative analysis of GPX4 immunofluorescence intensity in HGC-27 cells. (H) Quantitative analysis of GPX4 immunofluorescence intensity in AGS cells. Scale bar, 50 μm. (I) Western blot analysis of PIN1 and CPEB1 knockdown in HGC-27 cells. (J) Western blot analysis of PIN1 and CPEB1 overexpression in AGS cells. Data are presented as mean ± SD (n=3). *P<0.05; **P<0.01; ***P<0.001. PIN1, peptidyl-prolyl cis/trans isomerase 1; GC, gastric cancer; si, small interefering; ov, overexpression; CPEB1, cytoplasmic polyadenylation element-binding protein 1; NC, negative control; RT-qPCR, reverse transcription-quantitative PCR analysis; GPX4, glutathione peroxidase 4.

(60 mg/kg) was administered intraperitoneally once daily after tumors reached 100 mm^3. After 15 days of treatment, both erastin treatment and PIN1 knockout resulted in significant reductions in tumor burden, as evidenced by decreases

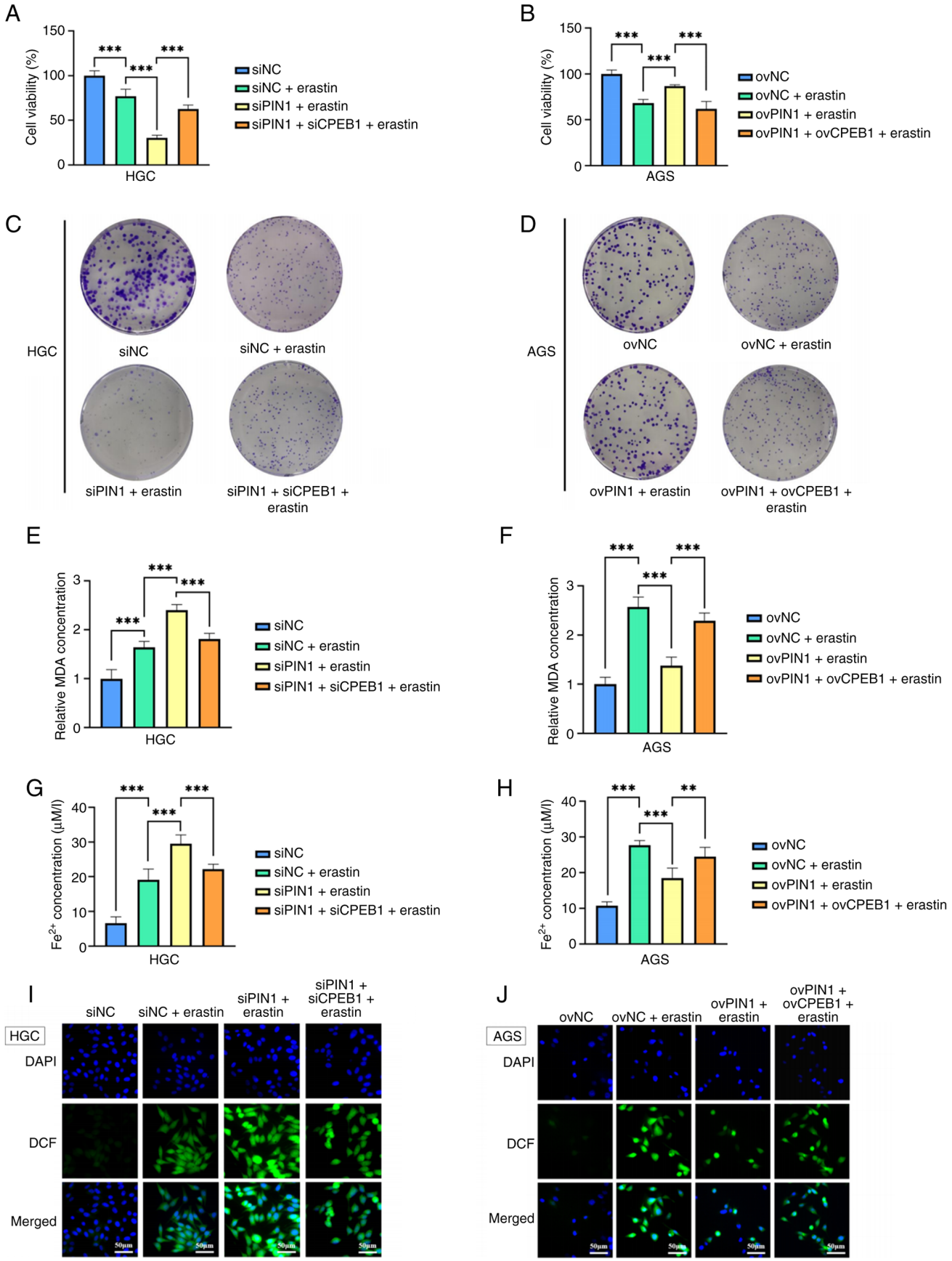

Figure 6. Regulation of ferroptosis in GC cells by PIN1 through CPEB1. Cell viability was assessed by Cell Counting Kit-8 assay in co-transfected (A) HGC-27 and (B) AGS cells. Colony formation assay for proliferation in co-transfected (C) HGC-27 and (D) AGS cells. MDA levels in co-transfected (E) HGC-27 and (F) AGS cells. Ferrous ion (Fe^{2+}) levels in co-transfected (G) HGC-27 and (H) AGS cells. Reactive oxygen species detected by 2',7'-dichlorodihydrofluorescein diacetate fluorescence intensity in (I) HGC-27 and (J) AGS cells. Data are presented as mean ± SD (n=3). $^{**}P<0.01$; $^{***}P<0.001$. PIN1, peptidyl-prolyl cis/trans isomerase 1; GC, gastric cancer; si, small interfering; ov, overexpression; CPEB1, cytoplasmic polyadenylation element-binding protein 1; NC, negative control; MDA, malondialdehyde.

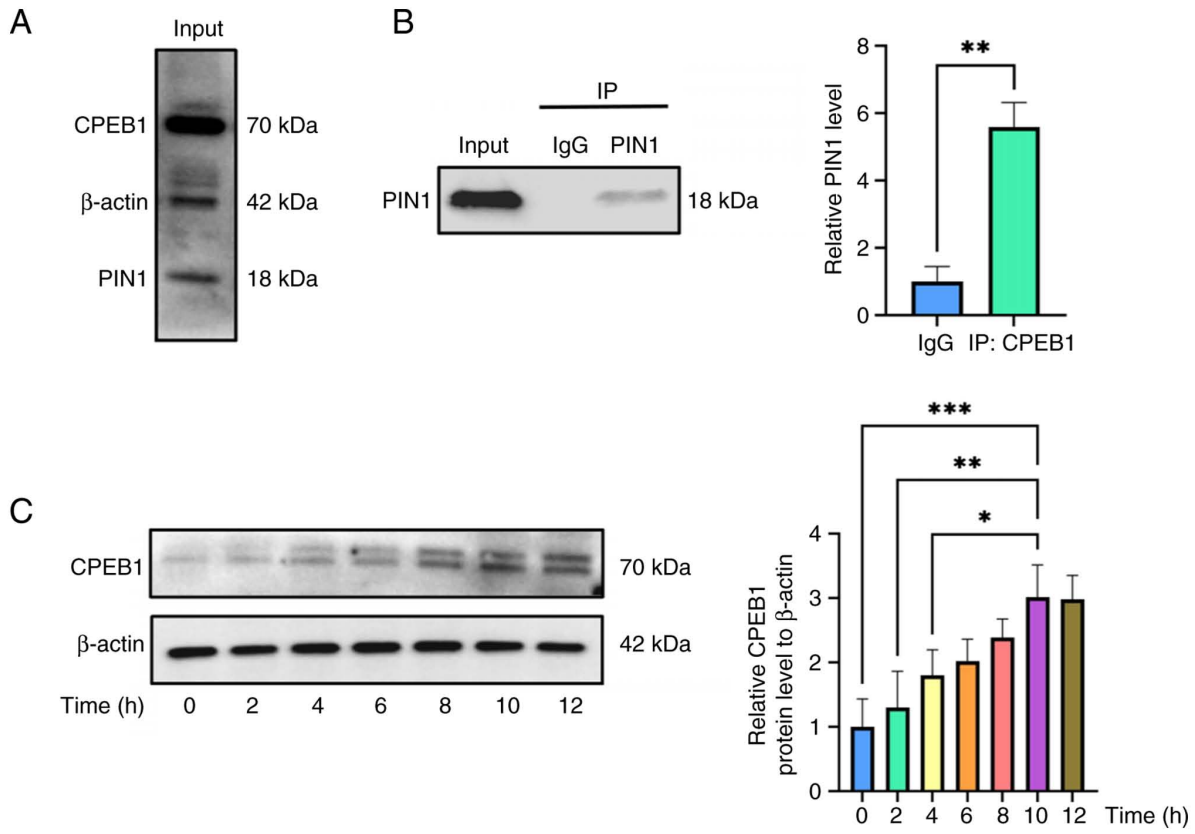

Figure 7. PIN1 interacts with CPEB1 and regulates its proteasomal turnover. (A) Input controls for CPEB1, PIN1 and β-actin in HGC-27 cell lysates. (B) Co-immunoprecipitation analysis of the endogenous interaction between PIN1 and CPEB1 in HGC-27 cells. (C) Western blot analysis of CPEB1 protein expression levels in HGC-27 cells treated with the proteasome inhibitor MG132 for the indicated durations. Data are presented as mean ± SD (n=3). *P<0.05; **P<0.01; ***P<0.001. PIN1, peptidyl-prolyl cis/trans isomerase 1; GC, gastric cancer; si, small interfering; ov, overexpression; CPEB1, cytoplasmic polyadenylation element-binding protein 1; NC, negative control; MDA, malondialdehyde.

in tumor volume and mass compared with the control groups (Fig. 8B-D). H&E staining revealed pathological mitotic figures in tumor cells (Fig. 8E).

To investigate whether ferroptosis suppresses the *in vivo* tumorigenic potential of GC cells, ferroptosis-related markers, including reactive ROS, MDA and Fe^{2+}, were analyzed in tumor tissues from the koNC + Erastin and koPIN1 groups using assay kits. The results revealed a significant increase in all three markers in both groups (Fig. 8I-K). Western blot analysis indicated that erastin treatment significantly reduced GPX4 protein levels, whereas PIN1 knockout increased CPEB1 expression and decreased GPX4 levels (Fig. 8H). These findings confirm that both PIN1 knockout and erastin treatment may induce ferroptosis and inhibit GC tumor growth *in vivo*.

Discussion

Ferroptosis is a distinct form of non-apoptotic cell death characterized by iron-dependent lipid peroxidation, driven by the catalytic activity of divalent iron or lipoxygenases, ultimately resulting in cellular damage and death (4). Due to elevated iron requirements, tumor cells are particularly vulnerable to ferroptosis under conditions of increased iron availability. As a result, induction of ferroptosis has emerged as a promising strategy to limit cancer progression and improve therapeutic outcomes (25). The present study shows that, in GC cells, PIN1 regulates ferroptosis by suppressing CPEB1, thus modulating GPX4 expression and increasing sensitivity to erastin-induced ferroptosis.

PIN1 is a prolyl isomerase that regulates the activity of multiple signaling proteins by catalyzing *cis*-trans isomerization of proline residues within phosphorylated motifs. Elevated PIN1 expression has been reported in numerous malignancies, where it functions as a key oncogenic factor (26). Although PIN1 has been associated with the regulation of ferroptosis in cervical cancer, the underlying molecular mechanisms remain unclear (15). In the present study, GC cell models with PIN1 knockdown or overexpression were established to investigate its role in ferroptosis. PIN1 deficiency increased erastin-induced ferroptosis, an effect reversed by treatment with Fer-1. Furthermore, even in the absence of ferroptosis inducers, PIN1 knockdown led to increased levels of ferroptosis-associated markers, including ROS, MDA and Fe^{2+}. *In vivo,* a subcutaneous xenograft model using HGC-27 cells demonstrated that both PIN1 knockdown and erastin treatment suppressed tumor growth, supporting the pro-ferroptotic and tumor-suppressive effects of PIN1 depletion.

Previous work has identified CPEB1 as a regulator of ferroptosis in GC, showing that CPEB1 enhances erastin-induced ferroptosis by downregulating GPX4 via Twist1 inhibition (27). Building on previous evidence that PIN1 binds to CPEB1 and promotes its ubiquitin-proteasome degradation (22,23), the interaction and regulatory mechanism were confirmed

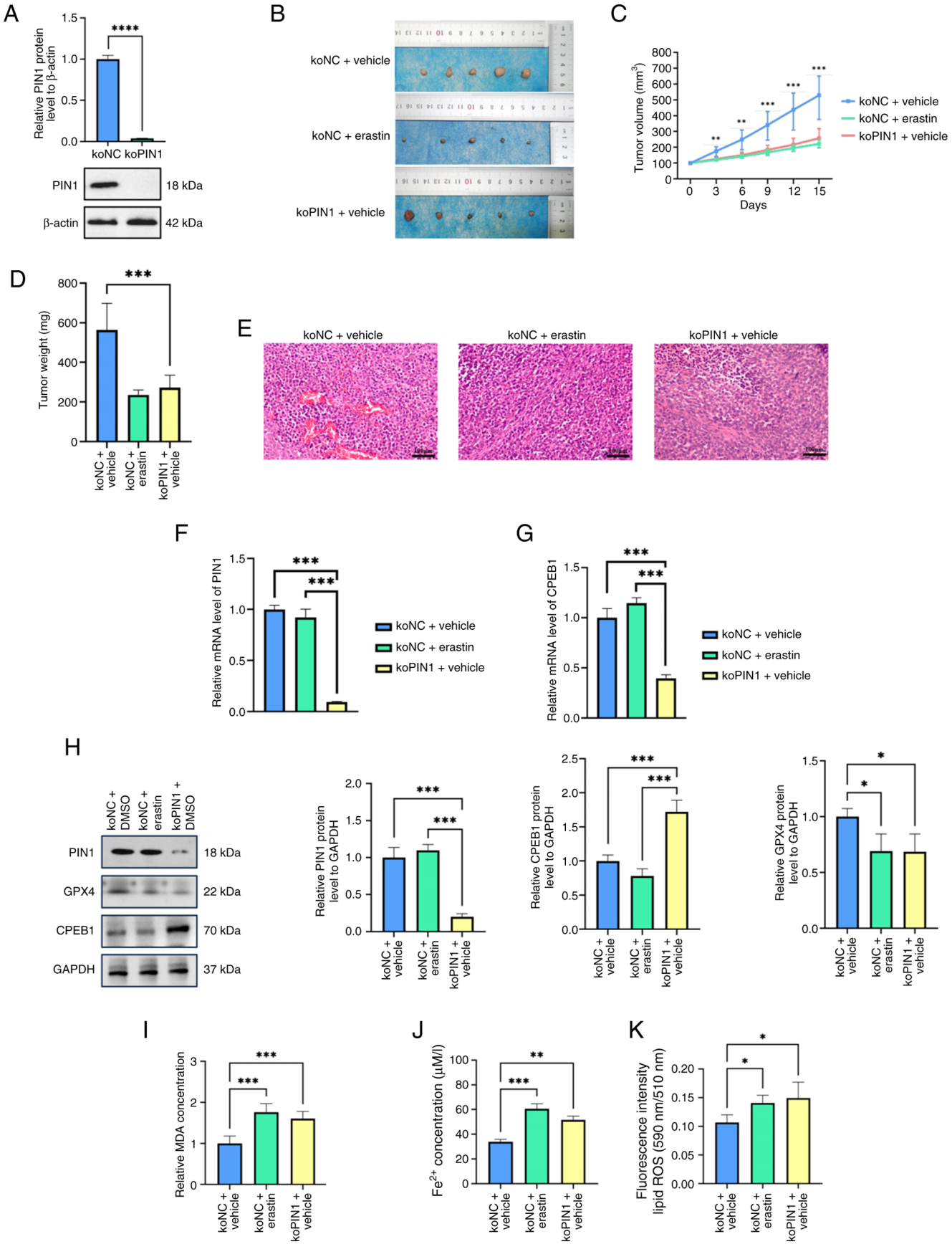

Figure 8. Anti-tumor effects of PIN1 knockdown in a xenograft model. (A) Western blot analysis of PIN1 knockout in HGC-27 cells prior to implantation. (B) Representative images of excised tumors. (C) Tumor volume. (D) Tumor weight. (E) H&E staining of tumor sections. Scale bar, 100 μm. (F and G) Revers e-transcription-quantitative PCR analysis of (F) PIN1 and (G) CPEB1 mRNA expression levels. (H) Western blot analysis of PIN1, GPX4 and CPEB1 protein levels. Levels of (I) malondialdehyde (MDA) (J) ferrous ion (Fe^{2+}) and (K) reactive oxygen species in tumor tissues. Data are presented as mean ± SD (n=5). *P<0.05; **P<0.01; ***P<0.001; ****P<0.0001. PIN1, peptidyl-prolyl cis/trans isomerase 1; GC, gastric cancer; si, small interfering; ov, overexpression; CPEB1, cytoplasmic polyadenylation element-binding protein 1; NC, negative control; MDA, malondialdehyde; GPX4, glutathione peroxidase 4; ko, knockout.

for the first time in gastric cancer cells in the present study, to the best of our knowledge. The data confirm endogenous interaction between PIN1 and CPEB1 and show that CPEB1 protein stability is regulated by the proteasomal pathway in GC cells. These results provide a mechanistic basis for the inverse relationship observed between PIN1 and CPEB1 protein levels in the functional models.

Based on this, the functional consequence of this axis in ferroptosis was investigated. Silencing CPEB1 in PIN1-deficient cells partially reversed ferroptosis and restored GPX4 expression. CPEB1 overexpression in PIN1-overexpressing cells attenuated the anti-ferroptotic effects of PIN1. These results support a model wherein PIN1 modulates ferroptosis in GC cells by interacting with and promoting the turnover of CPEB1, regulating the CPEB1-GPX4 axis.

Although direct ubiquitination assays were not performed, cellular data indicate that PIN1 primarily regulates CPEB1 at the protein level, with minimal alterations in mRNA expression, consistent with a mechanism involving PIN1-mediated ubiquitin-proteasome degradation. In animal models, PIN1 knockout led to reduced CPEB1 mRNA levels despite increased protein expression. This apparent difference may point to an additional layer of regulation involving mRNA stability. PIN1 has been reported to regulate RNA-binding proteins such as AUF1 (28) and AUF1 has been shown to promote the decay of CPEB1 transcripts in neuronal cells (29). These results suggest that PIN1 regulates CPEB1 through dual mechanisms, including post-translational control and indirect modulation of mRNA stability, underscoring the complexity of this regulatory network. This observation also suggests that, in addition to ubiquitination, PIN1 may affect CPEB1 expression through indirect mechanisms, such as modulation of transcription factor activity, mRNA turnover or epigenetic control. Furthermore, PIN1 is known to contribute to tumor microenvironment remodeling and metabolic reprogramming. The observed tissue-specific regulatory discrepancies may reflect intricate signaling interactions within the tumor microenvironment, although the precise mechanisms remain to be fully elucidated (30).

Clinical data from 27 patients with GC confirmed PIN1 overexpression, with a high ΔPIN1 score significantly correlating with aggressive pathological features, including lymphovascular invasion and perineural invasion. These findings suggest a key role for PIN1 in promoting local invasion in GC. This observation aligns with findings in T-cell acute lymphoblastic leukemia, where PIN1 enhances invasiveness by activating NOTCH3 (31); however, the specific downstream signaling mechanisms in GC remain unclear. The diagnostic performance of PIN1 and CPEB1 further supports the clinical relevance of this regulatory axis.

The present study has certain limitations that should be considered when interpreting the findings. Although the PIN1-CPEB1 interaction and proteasome-dependent regulation of CPEB1 were confirmed, direct evidence that PIN1 promotes polyubiquitination of CPEB1 in GC cells remains to be established using dedicated ubiquitination assays. Such experiments would strengthen the mechanistic definition of the post-translational regulatory pathway. With respect to the *in vivo* tumor-suppressive effect of PIN1 knockout, the present study did not determine whether this phenotype is solely due to restored CPEB1 activity, as rescue experiments re-expressing CPEB1 in PIN1-deficient tumors were not performed. Finally, the clinical associations observed in this single-center cohort of 27 patients require validation in larger, multi-center studies to ensure robustness and generalizability.

In conclusion, these findings define a regulatory axis in GC in which PIN1 interacts with CPEB1 and promotes its proteasome-dependent turnover. This regulation alleviates CPEB1-mediated suppression of GPX4, limiting ferroptosis and supporting tumor survival. The experimentally validated PIN1-CPEB1-GPX4 axis provides a mechanistic foundation for exploring PIN1 as a therapeutic target to sensitize GC to ferroptosis-inducing therapies. From mechanistic insight to clinical validation, the consistent overexpression of PIN1 and its association with invasive pathological phenotypes highlight its value as a potential therapeutic target. Therefore, the present findings, including the anti-tumor effect of PIN1 knockout *in vivo*, support exploring PIN1 as a therapeutic target. The combination of PIN1-targeted agents with ferroptosis inducers represents a potential strategy for GC and warrants further preclinical investigation. It should be noted that the current *in vivo* effect was based on genetic ablation; thus, the efficacy of pharmacological PIN1 inhibition in GC requires further evaluation using specific inhibitors.

Acknowledgements

Not applicable.

Funding

This work was supported by the Basic Scientific Research Operating Expenses of Provincial Universities in Heilongjiang Province (grant no. 2024-KYYWF-0462), the Young Science and Technology Talents Team Project of Chunyan Plan of Heilongjiang Province (grant no. CYQN24028) and the Mudanjiang City Key Research and Development Program (grant no. HA25CR062).

Availability of data and materials

The data generated in the present study may be requested from the corresponding author. The GSE220917 and TCGA-STAD datasets analyzed during the present study are available in the GEO (https://www.ncbi.nlm.nih.gov/geo/query/acc.cgi?acc=GSE220917) and TCGA (https://portal.gdc.cancer.gov/projects/TCGA-STAD) repositories, respectively.

Authors' contributions

AZ and TW designed and performed the research and drafted the manuscript. JS, QY, YJ and PZ contributed essential reagents and materials. JS collected clinical tissue samples. QY participated in the animal experiments. YJ performed the cell culture experiments. PZ performed the statistical analysis and prepared the tables and figures. LZ and LC analyzed the data. AZ and TW confirm the authenticity of all the raw data. JW and SR provided supervision and were responsible for manuscript review and editing. All authors read and approved the final manuscript.

Ethics approval and consent to participate

The animal study was approved by the Institutional Animal Care and Use Committee of Mudanjiang Medical University, Mudanjiang, China (approval no. IACUC-20240719-079). The use of human gastric cancer tissues was approved by the Medical Ethics Committee of Mudanjiang Medical University, Mudanjiang, China (approval no. 2023-MYGZR01). Written informed consent was obtained from all patients.

Patient consent for publication

Not applicable.

Competing interests

The authors declare that they have no competing interests.

References

1. Bray F, Laversanne M, Sung H, Ferlay J, Siegel RL, Soerjomataram I and Jemal A: Global cancer statistics 2022: GLOBOCAN estimates of incidence and mortality worldwide for 36 cancers in 185 countries. CA Cancer J Clin 74: 229-263, 2024.
2. Racz K, Legner A, Böhme F and Sebesta C: Gastric cancer. Wien Med Wochenschr 173: 227-231, 2023 (In German).
3. Dixon SJ and Olzmann JA: The cell biology of ferroptosis. Nat Rev Mol Cell Biol 25: 424-442, 2024.
4. Dixon SJ, Lemberg KM, Lamprecht MR, Skouta R, Zaitsev EM, Gleason CE, Patel DN, Bauer AJ, Cantley AM, Yang WS, *et al*: Ferroptosis: An iron-dependent form of nonapoptotic cell death. Cell 149: 1060-1072, 2012.
5. Nguyen TPM, Alves F, Lane DJR, Bush AI and Ayton S: Triggering ferroptosis in neurodegenerative diseases. Trends Neurosci 48: 750-765, 2025.
6. Chen F, Kang R, Tang D and Liu J: Ferroptosis: Principles and significance in health and disease. J Hematol Oncol 17: 41, 2024.
7. Mortensen MS, Ruiz J and Watts JL: Polyunsaturated fatty acids drive lipid peroxidation during ferroptosis. Cells 12: 804, 2023.
8. Pascual G, Majem B and Benitah SA: Targeting lipid metabolism in cancer metastasis. Biochim Biophys Acta Rev Cancer 1879: 189051, 2024.
9. Viswanathan VS, Ryan MJ, Dhruv HD, Gill S, Eichhoff OM, Seashore-Ludlow B, Kaffenberger SD, Eaton JK, Shimada K, Aguirre AJ, *et al*: Dependency of a therapy-resistant state of cancer cells on a lipid peroxidase pathway. Nature 547: 453-457, 2017.
10. Tsoi J, Robert L, Paraiso K, Galvan C, Sheu KM, Lay J, Wong DJL, Atefi M, Shirazi R, Wang X, *et al*: Multi-stage differentiation defines melanoma subtypes with differential vulnerability to drug-induced iron-dependent oxidative stress. Cancer Cell 33: 890-904.e5, 2018.
11. Jeong J, Usman M, Li Y, Zhou XZ and Lu KP: Pin1-catalyzed conformation changes regulate protein ubiquitination and degradation. Cells 13: 731, 2024.
12. Lu Z and Hunter T: Prolyl isomerase Pin1 in cancer. Cell Res 24: 1033-1049, 2014.
13. Zhang ZZ, Yu WX, Zheng M, Liao XH, Wang JC, Yang DY, Lu WX, Wang L, Zhang S, Liu HK, *et al*: PIN1 inhibition sensitizes chemotherapy in gastric cancer cells by targeting stem cell-like traits and multiple biomarkers. Mol Cancer Ther 19: 906-919, 2020.
14. Wu W, Xue X, Chen Y, Zheng N and Wang J: Targeting prolyl isomerase Pin1 as a promising strategy to overcome resistance to cancer therapies. Pharmacol Res 184: 106456, 2022.
15. Zhang Z, Hu Q, Ye S and Xiang L: Inhibition of the PIN1-NRF2/GPX4 axis imparts sensitivity to cisplatin in cervical cancer cells. Acta Biochim Biophys Sin (Shanghai) 54: 1325-1335, 2022.
16. Zhao Z, He J, Qiu S, Wang L, Huangfu S, Hu Y, Wu Q, Yang Y, Li X, Huang M, *et al*: Targeting PLK1-CBX8-GPX4 axis overcomes BRAF/EGFR inhibitor resistance in BRAFV600E colorectal cancer via ferroptosis. Nat Commun 16: 3605, 2025.
17. Pascual R, Segura-Morales C, Omerzu M, Bellora N, Belloc E, Castellazzi CL, Reina O, Eyras E, Maurice MM, Millanes-Romero A and Méndez R: mRNA spindle localization and mitotic translational regulation by CPEB1 and CPEB4. RNA 27: 291-302, 2021.
18. Takahashi N, Franciosi F, Daldello EM, Luong XG, Althoff P, Wang X and Conti M: CPEB1-dependent disruption of the mRNA translation program in oocytes during maternal aging. Nat Commun 14: 416, 2023.
19. Nagaoka K, Fujii K, Zhang H, Usuda K, Watanabe G, Ivshina M and Richter JD: CPEB1 mediates epithelial-to-mesenchyme transition and breast cancer metastasis. Oncogene 35: 2893-2901, 2016.
20. Xu M, Fang S, Song J, Chen M, Zhang Q, Weng Q, Fan X, Chen W, Wu X, Wu F, *et al*: CPEB1 mediates hepatocellular carcinoma cancer stemness and chemoresistance. Cell Death Dis 9: 957, 2018.
21. Wang J, Wang T, Zhang Y, Liu J, Song J, Han Y, Wang L, Yang S, Zhu L, Geng R, *et al*: CPEB1 enhances erastin-induced ferroptosis in gastric cancer cells by suppressing twist1 expression. IUBMB Life 73: 1180-1190, 2021.
22. Schelhorn C, Martín-Malpartida P, Suñol D and Macias MJ: Structural analysis of the Pin1-CPEB1 interaction and its potential role in CPEB1 degradation. Sci Rep 5: 14990, 2015.
23. Nechama M, Lin CL and Richter JD: An unusual two-step control of CPEB destruction by Pin1. Mol Cell Biol 33: 48-58, 2013.
24. Livak KJ and Schmittgen TD: Analysis of relative gene expression data using real-time quantitative PCR and the 2(-Delta Delta C(T)) method. Methods 25: 402-408, 2001.
25. Yao L, Hou J, Wu X, Lu Y, Jin Z, Yu Z, Yu B, Li J, Yang Z, Li C, *et al*: Cancer-associated fibroblasts impair the cytotoxic function of NK cells in gastric cancer by inducing ferroptosis via iron regulation. Redox Biol 67: 102923, 2023.
26. Zhang J, Zhou W, Chen Y, Wang Y, Guo Z, Hu W, Li Y, Han X and Si S: Small molecules targeting Pin1 as potent anticancer drugs. Front Pharmacol 14: 1073037, 2023.
27. Caligiuri I, Vincenzo C, Asano T, Kumar V and Rizzolio F: The metabolic crosstalk between PIN1 and the tumour microenvironment. Semin Cancer Biol 91: 143-157, 2023.
28. Kumar R: Pin1 regulates parathyroid hormone mRNA stability. J Clin Invest 119: 2887-2891, 2009.
29. Oe S, Koike T, Hirahara Y, Tanaka S, Hayashi S, Nakano Y, Kase M, Noda Y, Yamada H and Kitada M: AUF1, an mRNA decay factor, has a discordant role in Cpeb1 expression. Biochem Biophys Res Commun 534: 491-497, 2021.
30. Shi Y, Liu M, Li M, Mao Y, Ma J, Long R, Xu M, Yang Y, Wang W, Zhou Y, *et al*: Discovery of potent PROTAC degraders of Pin1 for the treatment of acute myeloid leukemia. Chem Sci 15: 5027-5035, 2024.
31. Franciosa G, Diluvio G, Gaudio FD, Giuli MV, Palermo R, Grazioli P, Campese AF, Talora C, Bellavia D, D'Amati G, *et al*: Prolyl-isomerase Pin1 controls Notch3 protein expression and regulates T-ALL progression. Oncogene 35: 4741-4751, 2016.